



Numerical Simulation of the Flow Field around Generic Formula One

D. TienPhuc^{1, 2†}, G. ZhengQi¹ and C. Zhen¹

¹ State Key Laboratory of Advanced Design and Manufacture for Vehicle Body of Hunan University, Changsha 430082, China

² Faculty of Automotive Engineering, Industrial University of Ho Chi Minh City, Ho Chi Minh 700000, Vietnam

†Corresponding Author Email: dangtienphuc.ckd@gmail.com

(Received November 27, 2014; accepted January 17, 2015)

ABSTRACT

The steady Reynolds-Averaged Navier-Stokes (RANS) method with the Realizable $k - \varepsilon$ turbulence model was used to analyze the flow field around a race car (generic Formula One). This study was conducted using the ANSYS software package. The numerical simulations were conducted at a Reynolds number based on the race car model (14.9×10^6). The time-averaged velocity field, flow topology, velocity magnitude, static pressure magnitude and vortex regions of the flow fields are presented in this paper. The measurements were performed on the vertical and cross-sectional planes. The results are presented graphically, showing the main characteristics of the flow field around the whole race car, whereas most previous studies only mention the flow field around individual components of race cars. The Realizable $k - \varepsilon$ turbulence model results showed consistency with the valuable validation data, which helps to elucidate the flow field around a model generic Formula one race car.

Keywords: Numerical simulation; Vehicle aerodynamics; RANS equations; Race car; Flow field.

NOMENCLATURE

C_d	drag coefficient	W	width of the race car model
C_l	lift coefficient		
F_i	foci of recirculation regions	I_{y_p}	distance from the boundary to the centre of the adjacent control volume
H	height of the race car model	μ	dynamic viscosity
L	length of the race car model	ρ	density of the air
S_{iab}	stagnation points		
u_τ	friction velocity		

1. INTRODUCTION

Vehicle flows have been the subject of a great number of investigations for decades because of their influence on overall vehicle performance and aerodynamic characteristics. Especially for Formula One racing cars, the aerodynamic characteristics play a vital role in race car performance because race car engines and body styling have advanced towards their limits in innovation and optimization or are regulated in racing. Hucho (1998) concluded that understanding flow field structure and aerodynamic characteristics around vehicles is an effective approach to enhance vehicle performance. Advances in aerodynamics are partly reflected in the increase in speed (Zhang *et al.* 2006), improve the vehicle performance (Mestiri *et al.* 2014) and

aerodynamic performance is one of the most important factors to be developed (Kuya *et al.* 2009). Several studies on the aerodynamic characteristics of Formula One racing cars have been previously studied (Wright 1982, Dominy 1992, Agathangelou 1998). These studies revealed that aerodynamics have a significant effect on the performance of Formula One racing cars.

There have been numerous studies about Formula One race cars. Kellar *et al.* (1999) conducted an experimental computation to investigate the aerodynamic performance of a Formula One car front wheel. This study showed the wake characteristics of the wheel and concluded that a more symmetrical wake reduces wheel drag. Mears and Dominy (2004) conducted experimental and computational work on the wake of a 40% full-scale

exposed wheel of a racing car to investigate the flow field characteristics and drag force. The results demonstrated a front and rear jetting phenomena at the wheels and they concluded that the computational results corroborated well with the experimental results. Next, Huminic *et al.* (2009) performed a numerical study on the influence of the boundary conditions at the ground level on the main aerodynamic characteristics and forces of a race car (Formula One) for both stationary ground and moving belt cases. The steady state RANS method with Shear Stress Transport (SST) $k - \epsilon$ turbulence model was applied. The results showed that the wheels were responsible for approximately 40% of the aerodynamic drag of the race car for both cases and that both the front and rear wings have a contribution on the down force up to 70 %. Issakhanian *et al.* (2010) conducted an experiment using PIV measurements to describe the flow field around a 60% scale model of an isolated Formula One wheel. The results showed asymmetric longitudinal vortex structures behind the wheel for the reversed flow regions in the wheel wake and a wheel wake profile that is unlike previous experimental results and postulations.

In recent years, studies by Axerio-Cilies *et al.* (2012) investigated flow fields that were approximately 60% scale-isolated stationary and rotating Formula One wheels. The purpose of their studies were to evaluate various accuracies of turbulence closure and to identify the existence of large-scale flow features. In this reference, the use of steady and unsteady RANS and large eddy simulation (LES) were compared with the PIV experiment. They concluded that the Realizable $k - \epsilon$ turbulence model is the most accurate at predicting the vortex eccentricity, whereas the LES and SST turbulence models are most accurate at simulating intrinsic wake unsteadiness. Next, Axerio-Cilies and Gianluca (2012) conducted a PIV experiment and numerical study on the flow field around a 60% scale rotating isolated Formula One tire to compare the sensitivity of the wake to various steady and unsteady RANS models. Their studies indicated that the counter-rotating vortex core locations at a span-wise plane in the tire wake obtained using the unsteady SST $k - \epsilon$ turbulence model corresponds with the experimental results. Knowles *et al.* (2013) conducted an experimental study in a near wake of a Formula One wheel to investigate the flow structures in the presence of a Formula One car and isolated wheel. They concluded that the presence of the car was found to significantly alter the structure of the wheel wake compared with an isolated wheel. Wang *et al.* (2014) performed a numerical simulation and wind tunnel experiment to investigate the aerodynamic characteristics of three typical rear shapes. The Realizable $k - \epsilon$ turbulence model was employed to compute the aerodynamic forces, and the computational results were consistent with the experimental data.

Although experimental and numerical simulations studies exist, many are only concerned with the flow field and aerodynamic characteristics around

wheels or wings. Very few previous studies regarding the flow field around whole race cars (Formula One) have been published in the open source literature. Therefore, this paper aims to gain a better understanding of the flow field structure as well as aerodynamic characteristics around a generic Formula One by numerical simulation. In this paper, we use steady RANS equations to survey the flow field structures around the whole race car. The measurements were performed on the vertical and cross-sectional planes.

2. RACE CAR MODEL GEOMETRIC PARAMETERS AND COMPUTATIONAL DOMAIN

2.1 Race car Model Geometric Parameters

To describe the race car model used in the research process, we refer to Fig. 1. The full-scale model has a length, $L = 4350$ mm, height, $H = 945$ mm and width, $W = 1750$ mm. This is the actual size of a Formula One car. The author has built a basic model race car and simplified some of the race car parts (e.g., smoothing on both sides and the tread area of the wheels, smoothing the underbody, and removing other small parts). However, the model still ensures effectiveness in showing the crucial flow field structure and aerodynamic characteristics of the race car. In addition, Fig. 1 also shows the origin of the coordinate system. The X-axis is along the transverse direction (rotating wheels are around the X axis), the Y-axis is along the longitudinal direction and the Z-axis is along the vertical direction.

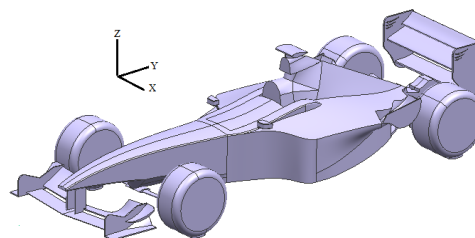


Fig. 1. Geometry of the race car model.

2.2 Computational Domain

Figure 2 shows the boundaries of the computational domain as a rectangular wind tunnel test section. To minimize the influence of the boundary conditions, the computational domain was designed with approximately seven times the width, six times the height, three car lengths from the input to the race car front and eight car lengths from the race car rear to the output of the model.

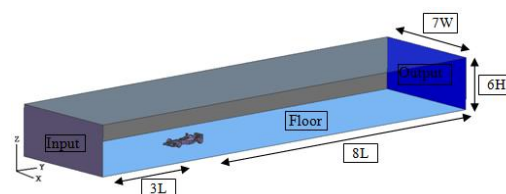


Fig. 2. Computational domain geometry.

The measurements were taken in the symmetry and cross-sectional planes. A schematic of the planes is shown in Fig. 3. For the symmetry planes, plane 1 was located at the race car center plane (y-z plane). Plane 2 was located at the rear view mirror center plane. Plane 3 was located at the tire center plane. In addition, the cross-sectional planes were taken perpendicular to the flow direction in the wake of the rear wing. Plane 4 was located at the rear wing (x-z plane). Two offset planes were 280 mm, 1000 mm from the rear wing plane 4 corresponding to plane 5, plane 6.

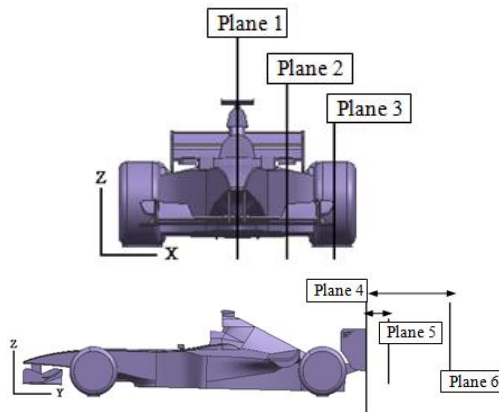


Fig. 3. Numerical simulation measurement planes.

3. NUMERICAL METHOD

3.1 Governing Equations and Discretization

The governing equations used in this paper are the steady RANS equations with the Realizable $k - \epsilon$ turbulence models selected to investigate the flow field around a race car. Because the mesh generation of the race car model is made up of tetrahedral meshes to provide more accurate results, we used the second-order accurate discretization scheme for the convective and viscous terms of the RANS. In the simulation process, we solve using the SIMPLE algorithm to solve the issue of the pressure-velocity coupling.

3.2 Convergence Criteria and Validation

The convergence criterion is dependent on the residuals of the turbulence model as well as aerodynamic coefficients (Strachan 2006). The residual of the turbulence model is one of the determinants of the numerical simulation error (Desai *et al.* 2008). In this paper, the convergence criteria of the solution were set lower than 10^{-4} . Details of the convergence criterion can be found in Kang *et al.* (2012) and Ansys .Inc. (2009).

Our paper studies the aerodynamic characteristics around the race car (open – wheel race car) because very little has been published regarding whole race cars in the open source literature. Racing teams are unwilling to share technical information with other racing teams and the technical information that is published refers to vehicles that are no longer competitive (Kieffer *et al.* 2006). Hence, the

validation of numerical results in this study uses C_d race car data published by Katz (1995). He showed that the drag coefficient (C_d) of a race car (generic F1) is 1.07.

3.3 Turbulence Modeling

In this study, the commercial CFD-code Ansys Fluent 12.0 was used for all of the simulations. Three turbulence models, including of RANS, the Realizable $k - \epsilon$, Shear-stress Transport (SST) $k - \omega$ and the Spalart-Allmaras (S-A) were tested. Each turbulence model had different calculation results; hence the choice of turbulent model in this study depends on the required level of accuracy.

A comparison between the C_d results (with 1,745,573 cells) obtained by using each turbulence model can be seen in Table 1. The Realizable $k - \epsilon$ turbulence model has the highest accuracy compared to the C_d in Katz. As we mentioned in the section 2.1, the race car model has simplified some of the race car parts, hence the drag coefficient is not larger than the data of Katz (1995). Table 1 shows that the Realizable $k - \epsilon$ turbulence model was selected in this study.

Table 1 The C_d results obtained by using each turbulence model

Turbulence model	Realizable $k - \epsilon$	SST $k - \omega$	Spalart-Allmaras	Data of Katz
Drag coefficient	0.986	1.154	1.187	1.07

3.4 Mesh Generation and Grid Independence Test

To analyze the flow field, it is necessary to split the flow domain into smaller subdomains, which is termed mesh generation. The mesh distribution of the longitudinal cross section of symmetry is shown in Fig 4a. The mesh topologies of the model are selected as an unstructured tetrahedral cell type, as shown in Fig. 4b. This type of mesh has been discussed in Knowles (2005).

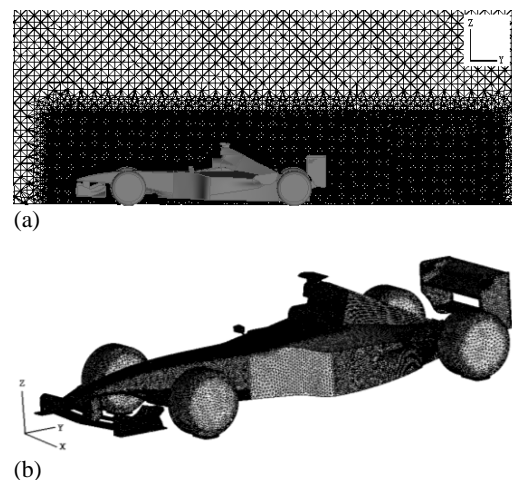


Fig. 4. Mesh distribution and topologies of the race car model.

In addition, to increase the accuracy of the calculated results, the grid of the model race car has been refined. In the refinement zones the cell size changes from 4 to 32 mm. The number of cells affects the calculated results, so we conducted a grid independence test. The criteria for selecting the number of cells is based on the C_d calculated compared to data of Katz, (1995) and computation time corresponding to each number of cells, which is tabulated in Table 2. The number of cells was determined as 2,541,914 cells (case 3) because the C_d value was found to be approximately equal to that of cases 4 and 5, but the number of cells and computation time are lower.

Table 2. Detailed grid size tests and C_d values

Cases	Number of cells	Drag coefficient	Computation time (h)
1	1,745,573	0.986	4
2	2,073,151	0.968	5
3	2,541,914	0.953	7
4	2,841,764	0.953	9
5	3,241,258	0.951	12

The flow across the surface of the vehicle creates a boundary layer around the wall surface of the vehicle. To observe this boundary layer, we used five prism layers that overlap at the wall surface of the model vehicle. The configuration of the prism layers are shown in Fig. 5.

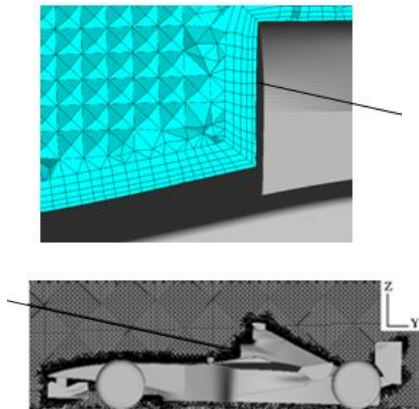


Fig. 5. Configuration of the prism layers at the wall surface of model.

To check the effectiveness of the grid, we first determined the value of y^+ , the non-dimensional length along the wall, given by

$$y^+ = \frac{\rho u_\tau y_p}{\mu} \quad (1)$$

The y^+ values are within the prescribed wall treatment. In this paper, we chose the y^+ values in the range of $30 < y^+ < 60$. These y^+ values are discussed further in Mears (2004).

3.5 Boundary Conditions

In the process of solving the numerical simulation, the surfaces of the cubic box (shown in Fig. 2) are set as follows: the input plane is considered to be a velocity-inlet where the airflow enters, the output

plane is considered to be a pressure-outlet where the airflow exits, the wind tunnel top wall and sidewalls are defined as no-slip walls and the floor is set as a moving wall. The gauge pressure for the pressure outlet boundary is set as zero Pascal. The wind speed, which effects the computation domain moving in the direction from input to output, is set to a speed of 50 m/s. The angular velocity of the rotating wheel matched the flow velocity of 159,033 rad/s. The numerical simulations were conducted at a Reynolds number based on the length of the race car model (14.9×10^6). The density of flow turbulence that moves and creates the input plane with the velocity-inlet is 0.2%. The density of flow turbulence that moves and creates the output plane with the velocity-inlet is 2%. The size of the hydraulic diameter (D_H), 7.752 (m), is calculated based on the following formula:

$$D_H = \frac{2(7W \times 6H)}{7W + 6H} \quad (2)$$

4. RESULTS

4.1 Time-Averaged Velocity Field

Figure 6 depicts the time-averaged patterns of streamlines and the magnitude of the velocity around the model race car in the vertical symmetry plane 1 (see Fig. 3 for the location of the plane). The colors indicate the flow field velocity through the plane from 0 to 60 m/s (darkest blue to darkest red). The velocity of the flow reduces as it reaches the front of the race car, then the velocity increases gradually but briefly decreases when it reaches regions 1 and 2.

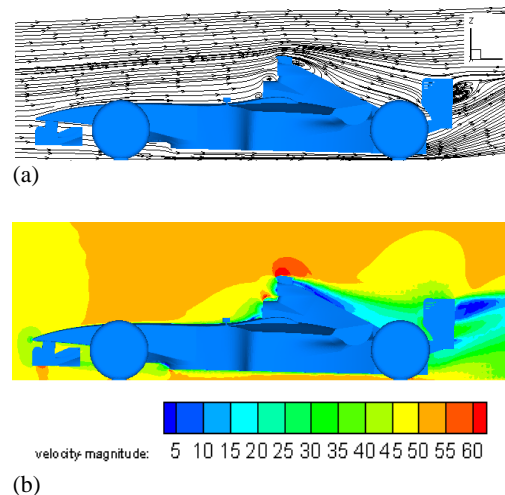


Fig. 6. Streamlines (a) and velocity magnitude (b) in vertical symmetry plane 1.

Once the flow moves over the top of the race car, the velocity reduces in the rear region due to the curvilinear nature of the rear geometry and the effect of the rear wing. Figure 7a focuses on the structure of the streamline flow above the race car body. Here, the centers of the foci and saddle points are designated as F and S, respectively. Three foci (F_1, F_2, F_3) can clearly be seen on the race car body,

which correspond to the locations that have a significant change of velocity magnitude. The domains of these foci depend on the size of the significant change velocity region. At the rear wing of the model, a recirculation region is formed (Fig. 7b). The recirculation region was generated by flow separation from the wing tip of the rear wing. Observing Fig. 7b, we see that the rear wing is not affected by the ground effect. These foci (F_4 , F_5 , F_6) with different domains are dependent on the angle of attack (AOA) of the aerofoils profile. Details of recirculation regions downstream of the rear wing can be found in Tsai *et al.* (2009), Jonathan and Tracie (2012). In addition, a saddle point S is developed in the wake region of the rear wing. The saddle point, S , shown in Fig. 7b, indicates the merging of two recirculation regions at the rear wing.

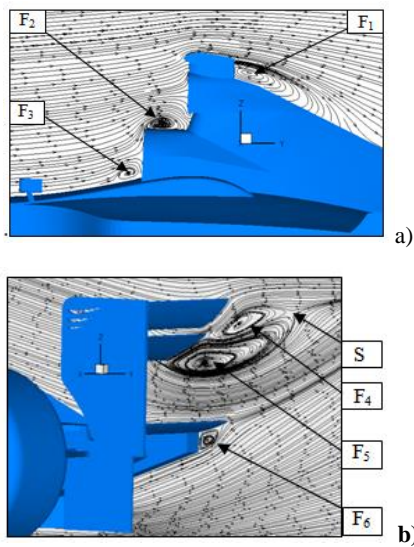


Fig. 7. The structure of the streamlines flow of the race car.

Figure 8 shows the time-averaged patterns of the streamlines and magnitude of the velocity around the rear view mirror in plane 2 (see Fig. 3 for the location of the plane). The incoming flow on the upstream of the rear view mirror is divided into upward and downward flows at the stagnation point, S_{1ab} , on the front face of the mirror. In addition, the upward flows are separated from corner A of the mirror, then reattached to the surface of the mirror because of the rounded leading mirror edge. The separation region is depicted in red, whereas the other regions are light colors. That means that the velocity magnitude at the separation zone is the largest. At the same time, the downward flows attach to the surface of the mirror at the lower side. In the downstream of the mirror, the recirculation region is identified. The focus F_7 occurs near the upper corner of the mirror in the downstream.

Figure 9 presents the time-averaged patterns of streamlines and velocity magnitude around the front wing in plane 2 (see Fig. 3 for the location of the plane). The front wing is one of the most important factors affecting the aerodynamic performance of open-wheel race cars (Zhang *et al.* 2006). The flow

streamlines on the downstream of the front wing tends to move upward and depends on the angles of attack (AOA) of the airfoil. Kieffer *et al.* (2006) concluded that the AOA of the airfoil has a considerable effect on the downward force of the front wing. By observing Fig. 9, we see that the velocity magnitude on the upper surface (the light color) of the wing is lower than the lower surface (the dark color) because of the ground effects on the wing. The features of the front wing in the ground effect are described by Kieffer *et al.* (2006) and Heyder-Bruckner (2011)

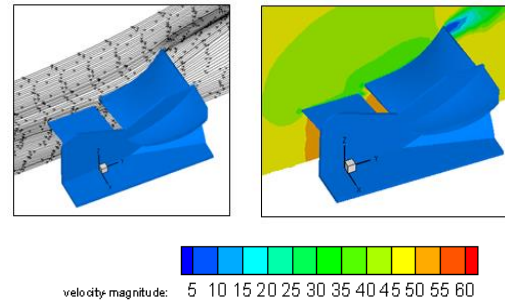


Fig. 9. Streamlines and velocity magnitude around the front wing in plane 2.

Next, the streamlines and velocity magnitude in plane 3 (see Fig. 3 for the location of the plane) around the front wheel (a) and rear wheel (b) are depicted in Fig. 10. The flow streamlines move in the Y direction. When the flow comes in contact with the wheel, the stagnation points, S_{2ab} and S_{3ab} , are formed. At that time, the flow separates into upward and downward flows and moves along the circular contour of the wheel. The velocity magnitude distribution reveals a low velocity region in front of the wheel as the flow reaches the stagnation point. Then, the velocity accelerates over the top of the wheel. Because this model is ideal for a race car (generic Formula One), it is not only affects the appearance of the positions of the stagnation points but also the velocity magnitude between the front and rear wheels. This has not been mentioned in previous studies that only studied isolated wheels.

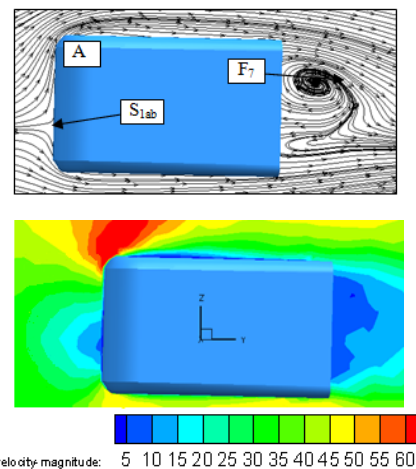


Fig. 8. Streamlines and velocity magnitude around the rear view mirror in plane 2.

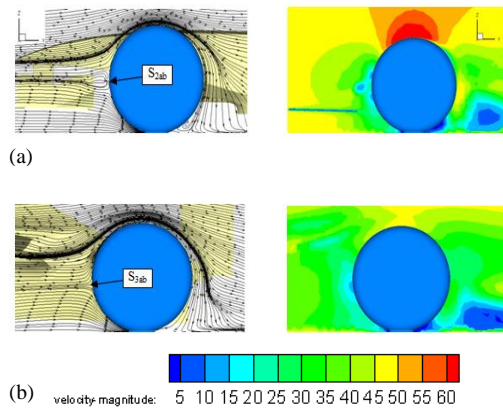


Fig. 10. Streamlines and velocity magnitude around the front wheel (a) and rear wheel (b) in plane 3.

The wake behind the race car is illustrated in Fig. 11, where the streamline patterns and magnitudes of the velocity are displayed in three *xz* cross-section planes (see Fig. 3 for the location of the plane). The wake is very symmetric as the race car itself is symmetric. Moreover, the streamline behind the race car in plane 4 is dominated by three pairs of rotating vortices (F_8, F_9, F_{10} and F_{11}, F_{12}, F_{13}). The vortices are separated and travel downstream of the race car. Observed in plane 4, the rotating trailing vortices (F_8, F_9 and F_{12}, F_{13}) originate from the bottom corners of the race car. The left and right rotating vortices show opposite rotational directions. At a location farther downstream of the race car, as shown for the different cross-section planes 5 and 6, the strong vortices only clearly appear from the upper corners of the rear wing and make outside fluid entrain into the node at the far wake (Kim *et al.* 2006). Hence, the rear wing also has a significant effect on the aerodynamic characteristics of a race car.

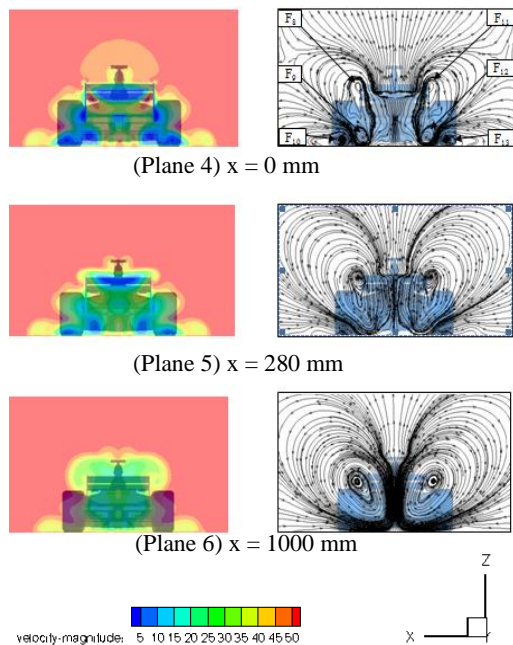


Fig. 11. Streamlines and magnitude of the velocity in three *xz* cross-sections of end-view planes.

4.2 Pressure Distribution

Table 3 The peak pressure coefficients of the race car for both cases

Peak pressure coefficient	Positive pressure	Negative pressure
Race car	1.709	-2.273

The changes in the flow separation over the race car can also affect the pressure distribution on the race car. The pressure coefficient distributions over the surface of the race car on the longitudinal symmetric plane are shown in Fig. 12. For more details, the differences between the values of the peak pressure coefficients are shown in Table 3.

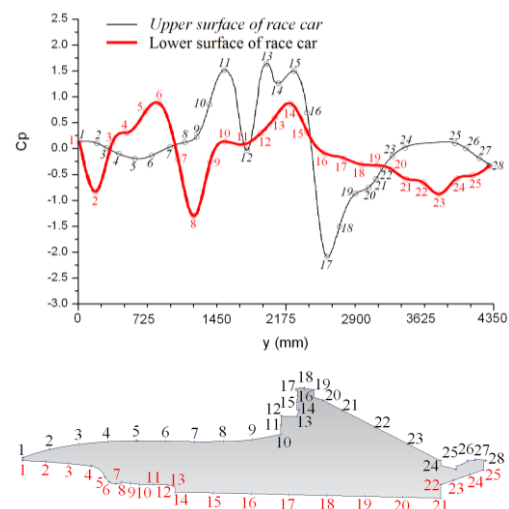


Fig. 12. Pressure coefficient distributions over the surface of the race car.

Figure 13 shows the static pressure distribution around and along the symmetry plane of the race car. The darkest red color shows areas of high pressure and the darkest blue color shows areas of lower pressure. According to Bernoulli's principle, it can be concluded that the places where the static pressure is lowest correspond to where the magnitude of the velocity is highest. As seen, the high static pressure regions (darkest red) in the front of the wheels, rear view mirror, nose cone and the upper of cockpit are created because the velocity magnitude slows down. Figure 13 also shows high static pressure created on the front and rear wheels but the front wheels were subjected to higher static pressure than the rear wheels. The pressure discrepancy between the front and rear regions of the race car generates a drag force.

5. CONCLUSION

This paper uses simulation methods to study the flow field around a race car (generic Formula one). Numerical simulation was conducted using the steady RANS method. Three turbulence models and grid independence were investigated. The Realizable $k - \epsilon$ turbulence model was selected in this study. The novelty of this paper is to help the reader understand the flow field around of the whole race car (generic Formula one) because most previous studies only examined the flow field

around the individual race car components. From the results of analysis using visual images, most of the features of the flow field were predicted, such as the separation points, saddle points, recirculation regions, and pressure distributions. The Realizable $k-\varepsilon$ turbulence model results were consistent with the data of Katz (1995), which helps to elucidate the flow field around a model generic Formula one.

To further explore this topic, we will perform experiments to investigate the aerodynamic characteristics of race cars in a wind tunnel in future studies.

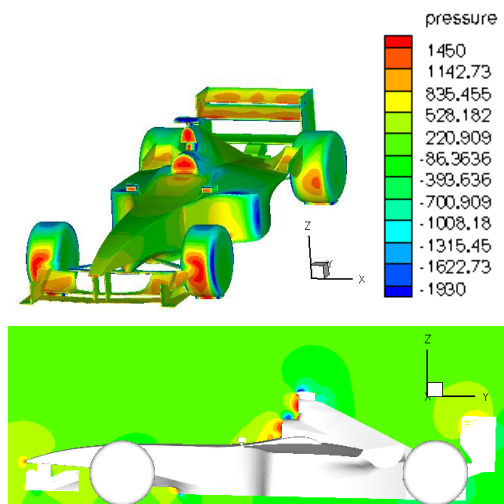


Fig. 13. Static pressure contours around and along the symmetry plane of the race car.

ACKNOWLEDGEMENTS

This work was accomplished by the supports of the State Key Laboratory of Advanced Design and Manufacturing for Vehicle Body, Hunan University, China.

REFERENCES

- Agathangelou, B. and M. Gascoyne (1998). Aerodynamic design considerations of a formula 1 racing car. *SAE Technical Paper* 980399
- Ansys inc., *Ansys Fluent 12.0 User's Guide*, Canonsburg, PA, 2009.
- Axerio-Cilies, J. and I. Gianluca (2012). An aerodynamic investigation of an isolated rotating formula 1 wheel assembly. *ASME J. Fluids Eng* 134(12), 121101.1-121101.16.
- Axerio-Cilies, J., E. Issakhanian, J. Jimenez and I. Gianluca (2012). An aerodynamic investigation of an isolated stationary formula 1 wheel assembly. *ASME J. Fluids Eng* 134 (2), 021101.1-021101.17.
- Desai, S., C. Lo and A. George (2008). A computational study of idealized bluff bodies, wheels, and vortex structures in ground effect. *SAE Technical Paper*.
- Dominy, R. G. (1992). Aerodynamics of Grand Prix Cars. *Proceedings of the Institution of Mechanical Engineers, Part D: Journal of Automobile Engineering* 206(4), 267-274.
- Fackrell, J. E. (1974). *The aerodynamic characteristics of an isolated wheel rotating in contact with the ground*. Ph. D. thesis, University of London.
- Heyder-Bruckner, J. (2011). *The aerodynamics of an inverted wing and a rotating wheel in ground effect*. Ph. D. thesis, University of Southampton, UK.
- Hucho, W. H. (1998). *Aerodynamics of road vehicles, 4th Ed.*, Society of Automotive Engineers.
- Huminic, A. and G. Huminic (2009). CFD Investigations of an Open-Wheel Race Car. *EASC 2009, 4th European Automotive Simulation Conference*, Munich, Germany.
- Issakhanian, E., J. E. Chris, P. L. Kin and K. E. John (2010). An experimental study of the flow around a formula one racing car tire. *ASME J. Fluids Eng.* 132(7), 071103.1-071103.8.
- Jonathan, W. V. and J. B. Tracie (2012). Ground effect phenomena about lift and downforce generating cambered aerofoils. *International Journal of Numerical Methods for Heat & Fluid Flow*, 22(2), 153 – 174.
- Kang, S. O., S. O. Jun, H. I. Park and *et al* (2012). Actively translating a rear diffuser device for the aerodynamic drag reduction of a passenger car. *International Journal of Automotive Technology* 13(4), 583-592.
- Katz, J. (1995). *Race car aerodynamics: Designing for speed*. Bentley Publishers, a division of Robert Bentley, USA.
- Kellar, W. P., S. R. G. Pearse and A. M. Savill (1999). Formula 1 car wheel aerodynamics. *Sports Engineering* 2(4), 203-212.
- Kieffer, W., S. Moujaes and N. Armbya (2006). CFD study of section characteristics of Formula Mazda race car wings. *Mathematical and Computer Modeling* 43(11-12), 1275-1287.
- Kim, J. S., S. Kim, J. Sung, J. S. Kim and J. Choi (1995). Effects of an air spoiler on the wake of a road vehicle by PIV measurements. *Journal of Visualization* 9(4), 411-418.
- Knowles, R. (2005). *Monoposto racecar wheel aerodynamics: investigation of near-wake structure and support-sting interference*. Ph. D. thesis, Cranfield University, UK.
- Knowles, R., J. S. Alistair and K. Kevin (2013). On the near wake of a Formula One front wheel. *Proc IMechE Part D: J Automobile Engineering*, 227(11), 1491–1502
- Kuya, Y., K. Takeda, X. Zhang, S. Beeton and T.

- Pandoleon (2009). Flow separation control on race car wing with vortex generators in ground effect. *ASME J. Fluids Eng.*, 131(12), 121102.1-121102.8
- Mestiri, R., A. Ahmed-Bensoltane, L. Keirsbulck, F. Aloui and L. Labraga (2014). Active Flow Control at the Rear End of a Generic Car Model Using Steady Blowing. *Journal of Applied Fluid Mechanics* 7(4), 565-571.
- Mears, A. and R. Dominy (2004). Racing Car Wheel Aerodynamics – Comparisons between Experimental and CFD Derived Flow-Field Data. *SAE Technical Paper* 2004-01-3555
- Mears, A. P. (2004). *The aerodynamic characteristics of an exposed racing car wheel*. Ph. D. thesis, Durham University.
- Russell, K. S. (2006). *The aerodynamic interference effects of side wall proximity on a generic car model*. PhD Thesis, Cranfield University, UK.
- Tsai, C., L. Fu, C. Tai, Y. Huang and J. Leong (2009). Computational aero-acoustic analysis of a passenger car with a rear spoiler. *Applied Mathematical Modelling* 33(9), 3661–3673.
- Wang, Y., Y. Xin, Zh. Gu, Sh. Wang, Y. Deng and X. Yang (2014). Numerical and Experimental Investigations on the Aerodynamic Characteristic of Three Typical Passenger Vehicles. *Journal of Applied Fluid Mechanics* 7(4), 659-671.
- Wright, P. G. (1982). The influence of aerodynamics on the design of formula one racing cars. *Int. J. Veh. Des.* 3(4), 383–397.
- Zhang, X., W. Toet and J. Zerihan (2006). Ground Effect Aerodynamics of Race Cars. *ASME J. Fluids Eng* 59(1), 33-49.